The Depth Dependent Damage Profile in Nickel Irradiated with Nickel or Copper Ions

J.B. Whitley, G.L. Kulcinski, P. Wilkes, and H.V. Smith, Jr.

July 1978

UWFDM-253

J. Nucl. Matls. 79, 159 (1979).

The Depth Dependent Damage Profile in Nickel Irradiated with Nickel or Copper Ions

J.B. Whitley, G.L. Kulcinski, P. Wilkes, and H.V.
Smith, Jr.

Fusion Technology Institute
University of Wisconsin
1500 Engineering Drive
Madison, WI 53706

http://fti.neep.wisc.edu

July 1978

UWFDM-253

J. Nucl. Matls. 79, 159 (1979).

The Depth Dependent Damage Profile in Nickel Irradiated with Nickel or Copper Ions

J.B. Whitley, G.L. Kulcinski, P. Wilkes, H.V. Smith, Jr.

July 1978

UWFDM-253

The Depth Dependent Damage Profile in Nickel Irradiated with Nickel or Copper Ions

J.B. Whitley, G.L. Kulcinski, P. Wilkes, H.V. Smith Jr.

Abstract

High purity nickel samples have been irradiated with high energy (>14 MeV) heavy ions and the resultant microstructure examined in cross section (i.e., in a plane parallel to the incident ions). The microstructure observed after irradiation with copper ions was not significantly different than that observed after nickel ion irradiation. Swelling near the ion end-of-range was less than that in the mid-range in both the self-ion and copper ion irradiated samples. A 100 nm void denuded zone was observed at the front surface in samples irradiated at 525°C, and voids were observed at depths ≈15% greater than the calculated damage curves. An irradiation at 200°C produced a loop lattice structure aligned along {001} with a spacing of ≈40 nm.

The steady-state rate equations were formulated and solved to give the depth dependent defect concentrations. The calculated void growth rate was found to qualitatively fit the experimental results. A depth dependent radiation enhanced diffusion model predicted the result that for ion fluences used in this study, the injected copper impurities were confined to the end-of-range region.

The Depth Dependent Damage Profile in Nickel Irradiated with Nickel or Copper Ions

J.B. Whitley, G.L. Kulcinski, P. Wilkes, and H.V. Smith, Jr.

1. Introduction

In the past several years, simulation studies have become a useful tool in the study of the swelling behavior expected from high fluence, high temperature neutron irradiated metals.[1,2] Comparison of the final damage microstructure produced by heavy-ions to that in a neutron irradiated sample is clouded by several unique aspects of the former such as surface effects or effects due to the limited volume of material irradiated.[3] In addition, an accurate theoretical description of the damage process at the high displacement rates typical of simulation studies has proven to be elusive.[4] Without a proper description of the effect of dose rate on the swelling response of a material, the usefulness of high displacement-rate simulation studies as an indicator of material response to neutron irradiation will be greatly reduced.

To expand our understanding of the radiation damage process caused by heavy-ions, this experiment used a sample preparation technique which allowed the direct cross sectional viewing of the microstructure along the ion path.[5] This powerful technique, which is a modification of the procedure first applied by Spurling and Rhodes[6] to proton irradiated stainless steel, allows a detailed study of the depth variation in the irradiated microstructure. In this paper, the effects of copper and nickel ion irradiations were compared. The steady-state rate equations for defect concentrations were solved to give their spatial profiles for comparison with the experimental damage profiles. The final concentration profile of the incident copper ions was calculated by applying an appropriate radiation enhanced diffusion model.[7]

2. Experimental Procedure

The material used in this study was Marz grade nickel obtained from Materials Research Corportation and of nominal purity 99.995% (substitutional impurities only). The sample lot analysis showed impurity levels of copper less than 3 wt-ppm. After machining the samples into the proper shape for irradiation, they were given a recrystallization anneal in an inert atmosphere for one hour at 1000°C and furnace cooled. The samples were then electropolished in a solution of 60% sulfuric acid with 40% water to give the cleanest possible surfaces prior to loading into the target chamber. The samples were then irradiated in a high temperature, ultra-high vacuum target chamber[8] using high energy copper or nickel ions (14 MeV to 19 MeV) accelerated by a tandem Van de Graaff accelerator.

The theoretical damage energy deposition rate as a function of depth was calculated using the updated version of the Brice code[9] which includes energy transport by secondary ions. The displacement energy was taken as 40 eV,[10] with the nuclear energy loss rate converted to displacements (i.e., dpa) using the ASTM standard.[11] An example of the results for 14 MeV nickel ions incident on a nickel target is shown in figure 1. The right-hand axis gives the displacement rate typical of the ion flux ($\sim 2\text{x}10^{12}$ ions/cm^2/s) used in this experiment. The depression of the curve near the front surface is due to energy transport by the secondary ions. There is approximately a factor of

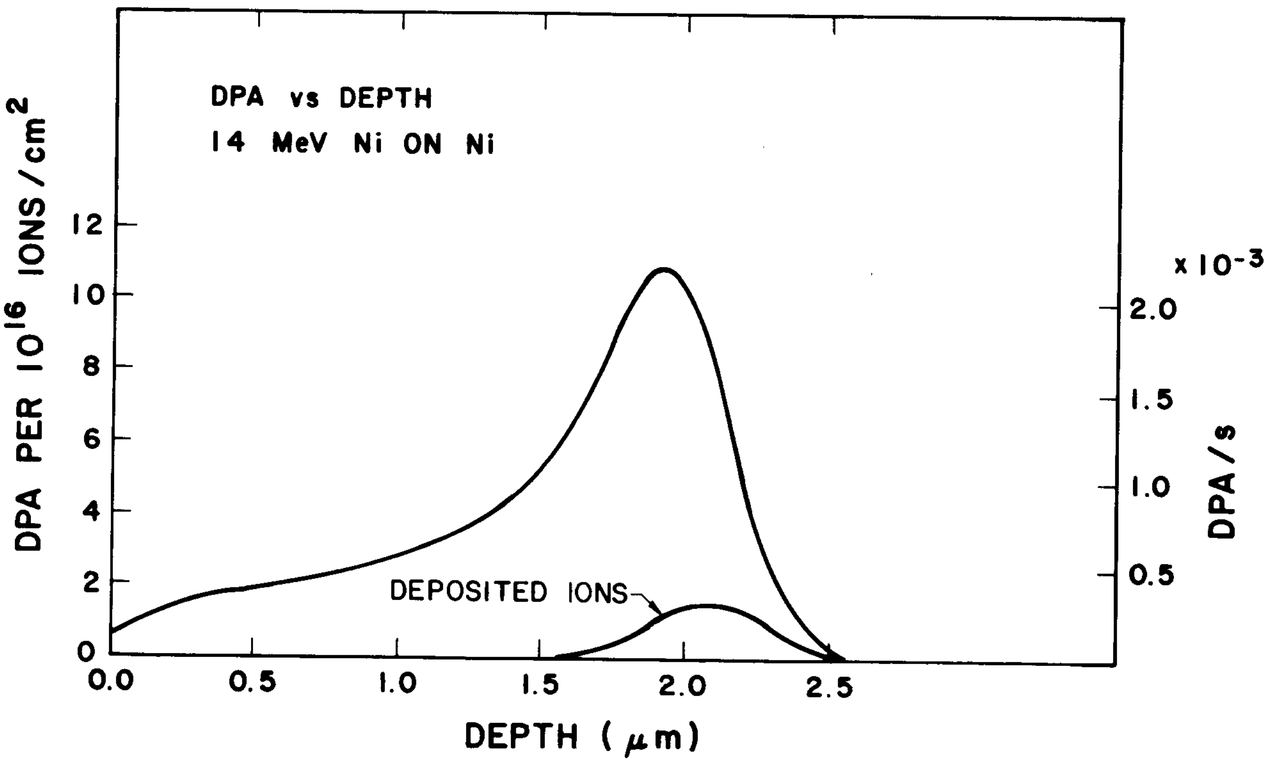

Figure 1. The displacement curve for 14 MeV nickel ions incident on nickel as predicted by Brice[9]. The right-hand axis gives the displacement rate corresponding to the ion flux (~2 x 10^{12} ions/cm^2/s) used in this experiment. Also shown in the relative distribution of the implanted ions.

ten variation in the total dose and the dose rate from the near surface region to the peak, with the peak of the displacement curve occurring at a depth of 1.9 μm. Also shown is the relative range distribution of the incident ions. The displacement damage curve for 14 MeV copper ions is very similar to figure 1, while the curve for 19 MeV copper ions has the same general shape and magnitude with the peak of the damage curve occurring at 2.4 μm.

After irradiation, the samples were prepared in cross section in a manner similar to Spurling and Rhodes[6] (fig. 2). The samples were first given an activation treatment in a solution of Wood's nickel(12) (60g $NiCl_2$, 31 ml HCl, 250 ml H_2O) by making the sample anodic for 20 seconds at a current density of 25 mA/cm^2. This step was necessary to remove the metal oxide layer and assure a good bond. The amount of material removed by this process was estimated to be less than 0.05 μm by interference microscopy. After activation, the current was reversed in this same solution and a thin nickel strike applied. The sample was then transferred directly to a high chlorine nickel plating solution containing 150 g $NiSO_4$, 150 g $NiCl_2$ and 50 g boric acid in 1000 ml H_2O. Plating for ≈24 hours in this solution at 50°C and a current density of 300 mA/cm^2 resulted in a final specimen thickness greater than 2 mm. The sample was then mounted in resin and sliced in cross section using a low speed diamond saw. Three millimeter discs were then cut from these slices and thinned for transmission electron microscopy (TEM) using a solution of 33% nitric acid, 67% methyl alcohol at -15°C in a twin jet electropolishing unit. The actual region of the disc that contains the damage is rather small as is shown schematically in figure 2. However, by careful alignment of the polishing unit at least one successful foil was usually obtained from the several slices produced from each irradiated region.

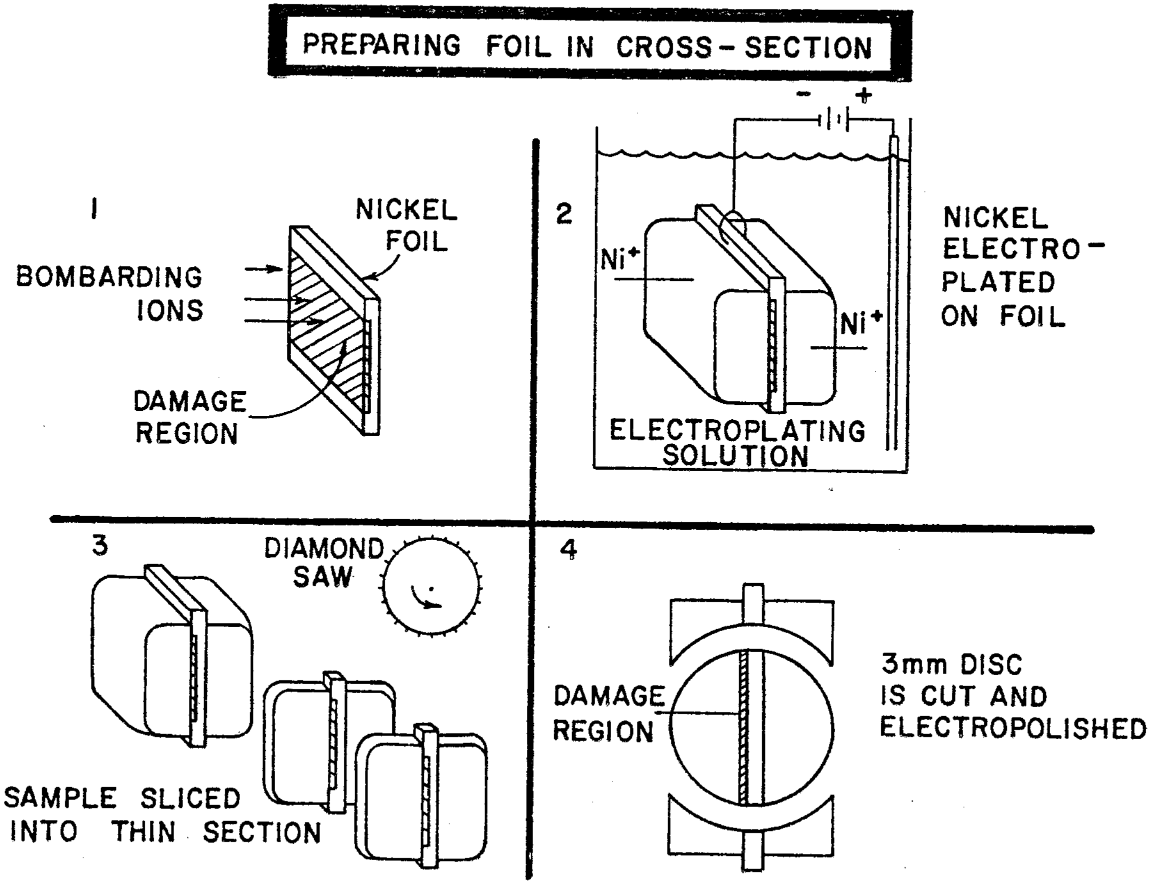

Figure 2. A schematic representation of the cross-section sample preparation procedure.

Analysis was carried out on a JEM 100B electron microscope operated at 120 kV. The depth distribution of the microstructure data was determined by dividing the micrograph into regions 0.25 μm wide parallel to the front surface. The foil thickness was determined using the standard stereo technique. Void size distributions were measured on a Zeiss comparator with swelling values calculated in a manner similar to Ryan.[10]

3. Experimental Results

The primary purpose of this study was a comparison of samples irradiated at 525°C to different fluence levels and using different ions. A typical micrograph obtained from a sample irradiated with 19 MeV copper ions to a fluence of 5×10^{15} ions/cm^2 and prepared in cross section is shown in figure 3. The original foil surface is visible at the left-hand-side of the micrograph, with the incident ions having travelled from left to right. Voids were observed to form quite readily in all samples even without prior helium injection. There is a definite denuded region at the front surface with very few voids observed closer than ≈ 100 nm from the surface. This denuded area was followed by a region ≈ 150 nm wide of unusually large voids. Over the next micrometer, the void density rises while void size drops. The voids throughout the damage region were truncated octahedra with the degree of truncation increasing slightly with depth. Near the end-of-range the void density drops rapidly. In all samples, voids were observed at depths ≈ 15% greater than the damage range predicted by Brice.[9]

A limited dose scan with total ion fluence ranging from 3×10^{15} to 1×10^{16} ions/cm^2 was carried out at 525°C with 19 MeV copper ions. The micrographs of figure 4 show the void microstructure development with dose. The void density in the end-of-range region is seen to increase with

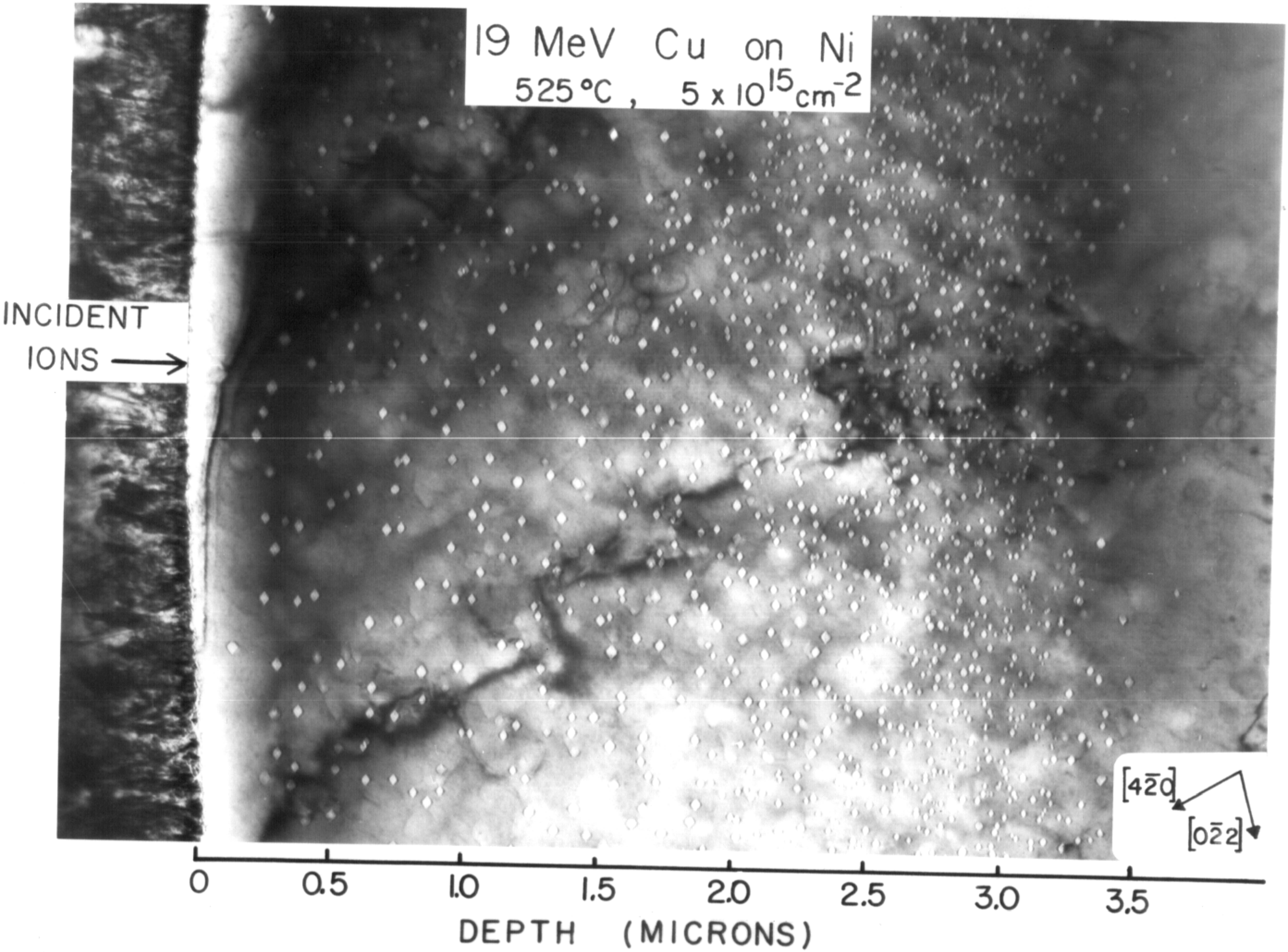

Figure 3. A micrograph of a nickel sample irradiated at 525°C with 19 MeV copper ions to a fluence of 5×10^{15} ions/cm^2 and prepared in cross-section.

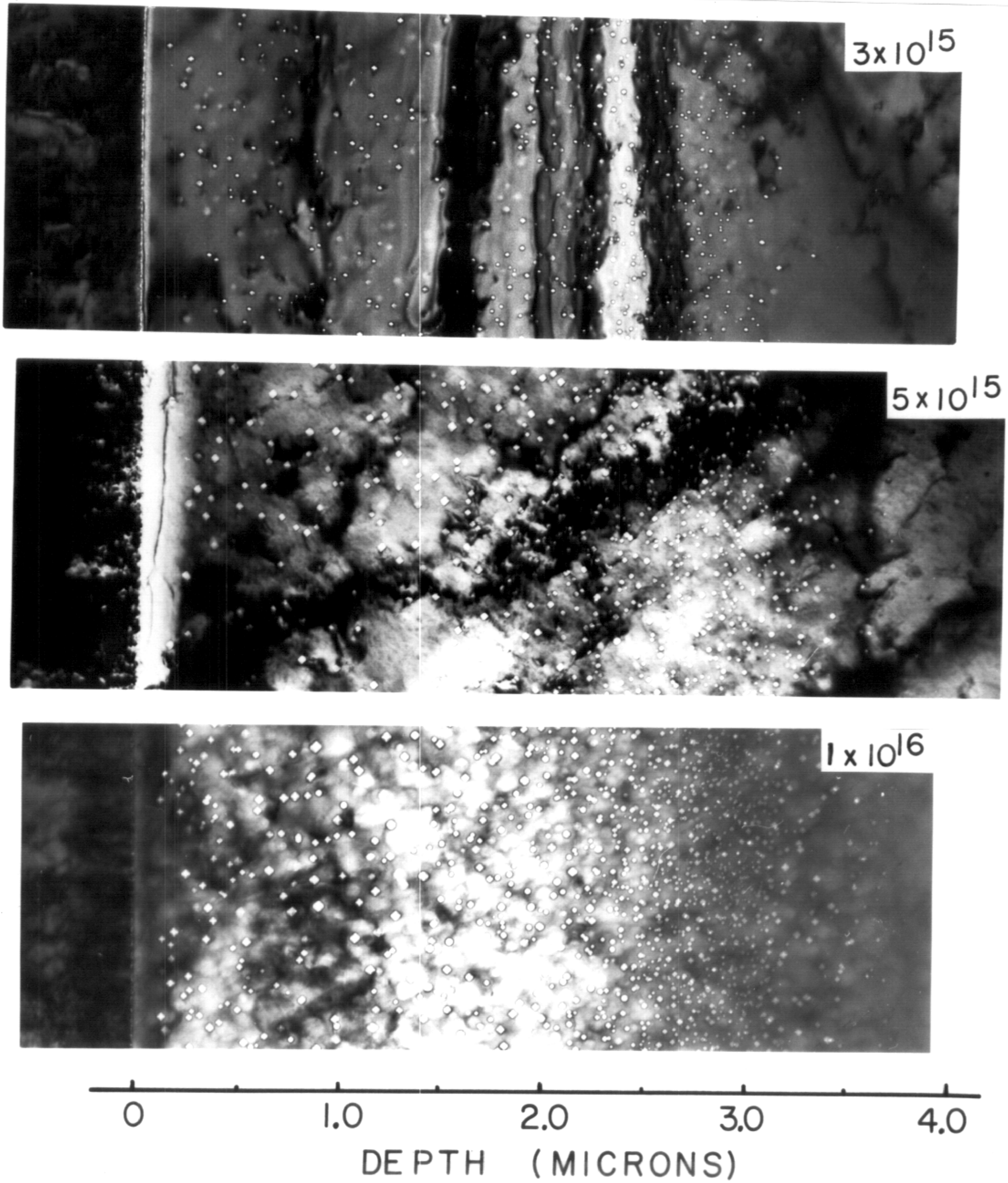

Figure 4. Micrographs of three nickel samples irradiated at 525°C with 19 MeV copper ions to the fluence levels (ions/cm^2) indicated on the micrographs.

increasing dose, with relatively few voids seen at depth of 3.6 μm in the low dose sample. The high dose sample, however, has a significant number in this region defining a rather sharp end-of-range. The variation from sample to sample showed the expected behavior with void size and void density increasing with increasing ion fluence.

Figure 5 shows the depth dependence of the void number densities determined for these samples using a 0.25 μm interval. Note that while the data would be strictly presented as a histogram, the presentation of the data was simplified by showing a single data point at the center of each depth interval and then drawing a smooth curve through the points to aid the eye in following data trends. In general, the void density curve follows the displacement curve rather closely. This result is not unexpected since the void nucleation rate is dose rate dependent. The void densities for the two high dose samples are the same within the experimental error indicating that the void density has saturated. This implies that the final void density at the end of nucleation is determined by the dose rate and not only by the total damage state.

To study the effects of irradiating with copper ions in the end-of-range region, irradiations were performed on samples given identical pre-irradiation treatments, and then irradiated at 525°C with either 14 MeV nickel ions or 14 MeV copper ions to a fluence of 1.3×10^{16} ions/cm^2 (i.e., ≈15 dpa at the peak). The void size, void number density and the void volume fraction measured from these samples as a function of depth are shown in figure 6. In general, there were no major differences observed between the two microstructures. The copper ion irradiated sample has a

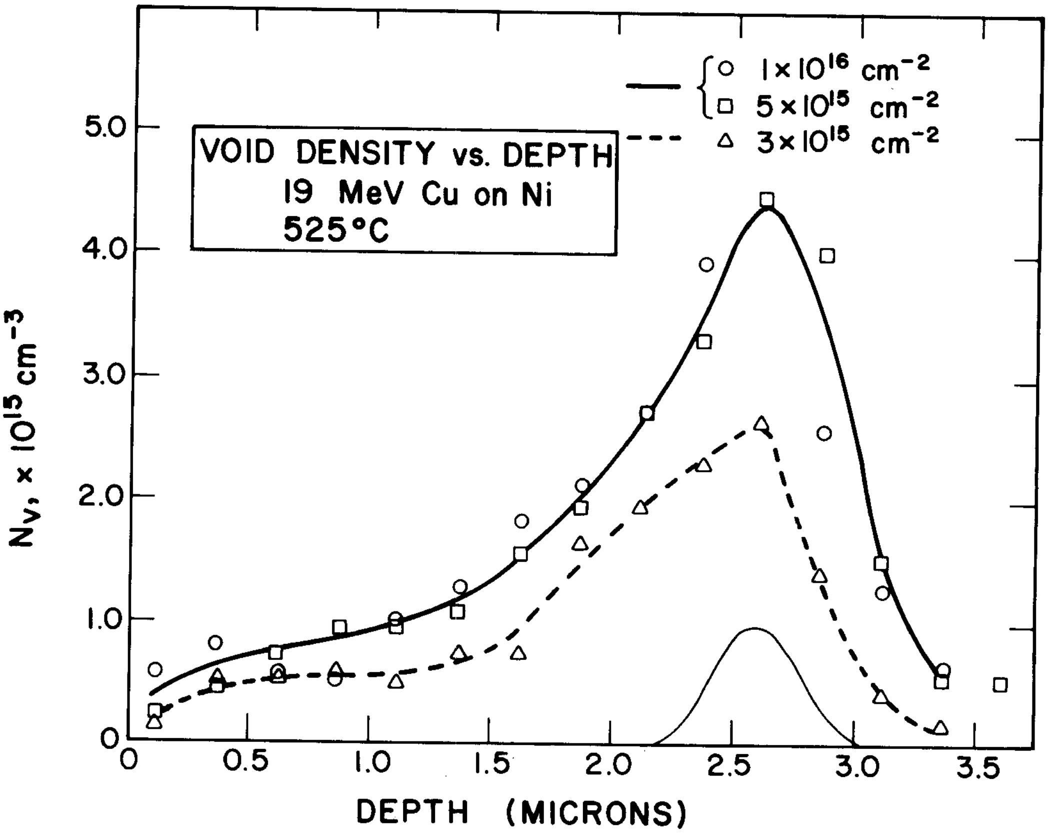

Figure 5. Void density (N_V) vs. depth for nickel irradiated at 525°C to three different fluence levels. The curves serve only to guide the eye. The depth distribution of the deposited ions is also included on the figure.

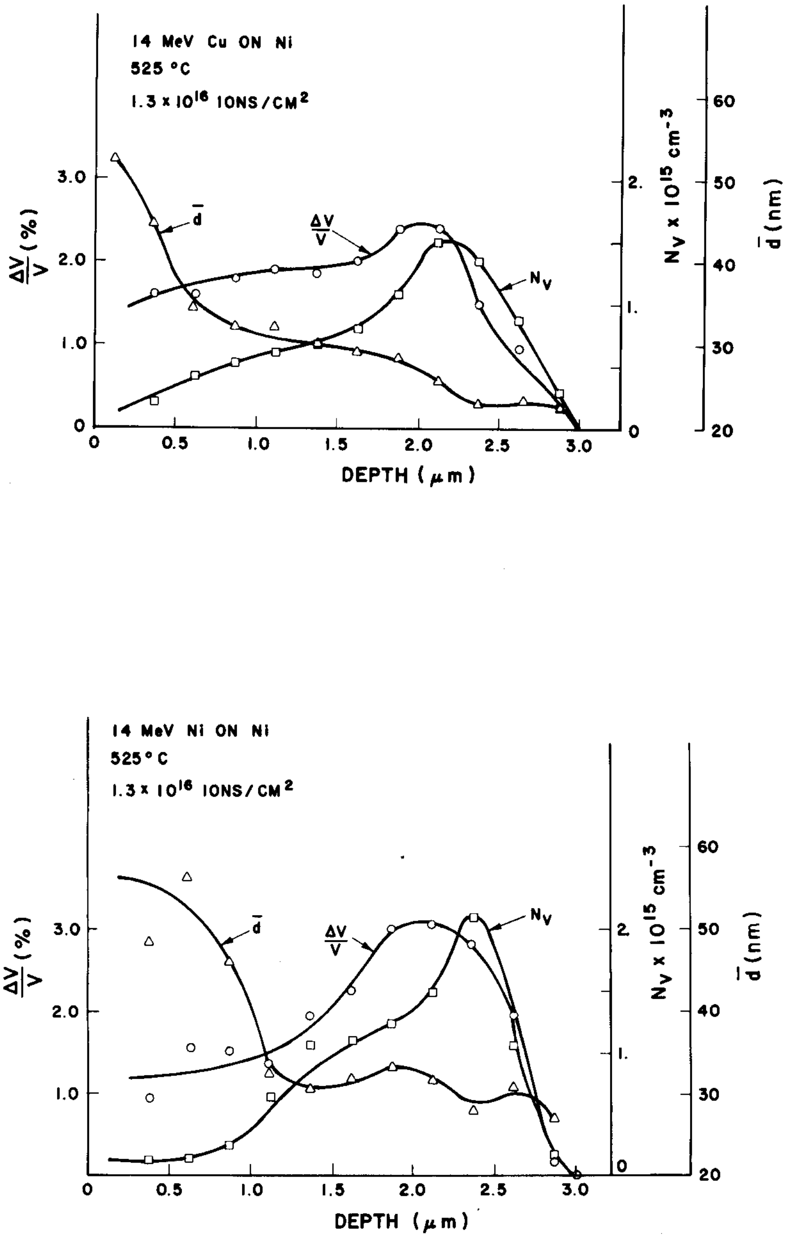

Figure 6. Void size, void density, and void volume as a function of depth in nickel irradiated at 525°C. a) After irradiation with 14 MeV copper ions, b) After irradiation with 14 MeV nickel ions. The ion fluence in each case was 1.3 x 10^{16} ions/cm^2.

lower void density and void size in the end-of-range region and this may be an indication of point defect interactions with the implanted copper ions. The magnitude of the reduction is rather small, however, indicating that the interaction is weak at these copper concentrations (≈2000 appm copper).

In figure 7, the swelling curves of figure 6 are shown plotted along with the displacement curve of figure 1. The end-of-range swelling values and the variations from mid-range to peak for the copper irradiated sample are lower than the values from the nickel irradiated sample. Note, however, that the variation in the swelling curve for the nickel irradiated sample is much smaller than the variation in the displacement curve in the equivalent depth range, indicating that even for self-ion irradiations, the final swelling profile is not always directly related to the total damage level.

The dislocation structure observed in these samples consisted of dense network dislocations interacting with the voids with a few dislocation loops scattered in the matrix. The typical dislocation structure near the end-of-range is shown in figure 8. The total dislocation densities in these samples were about 5×10^9 cm/cm^3 and did not vary strongly with depth.

An irradiation was also carried out at 200°C with 14 MeV nickel ions to study the development of the loop structure at low temperatures. A well-developed loop lattice formed along {100} directions with a spacing of ≈40 nm as is shown in figure 9. This result is consistent with several other low temperature nickel irradiations[13,14,15] except that the lowest temperature at which an aligned structure had been observed was 280°C. The loop structure in this study extended all the way to the foil surface without disordering. The loop lattice also extends well beyond the area of peak damage, and can be observed at depths of 3 μm. The loop lattice spacing is approximately constant throughout the damage region and hence does not vary with the local dose rate.

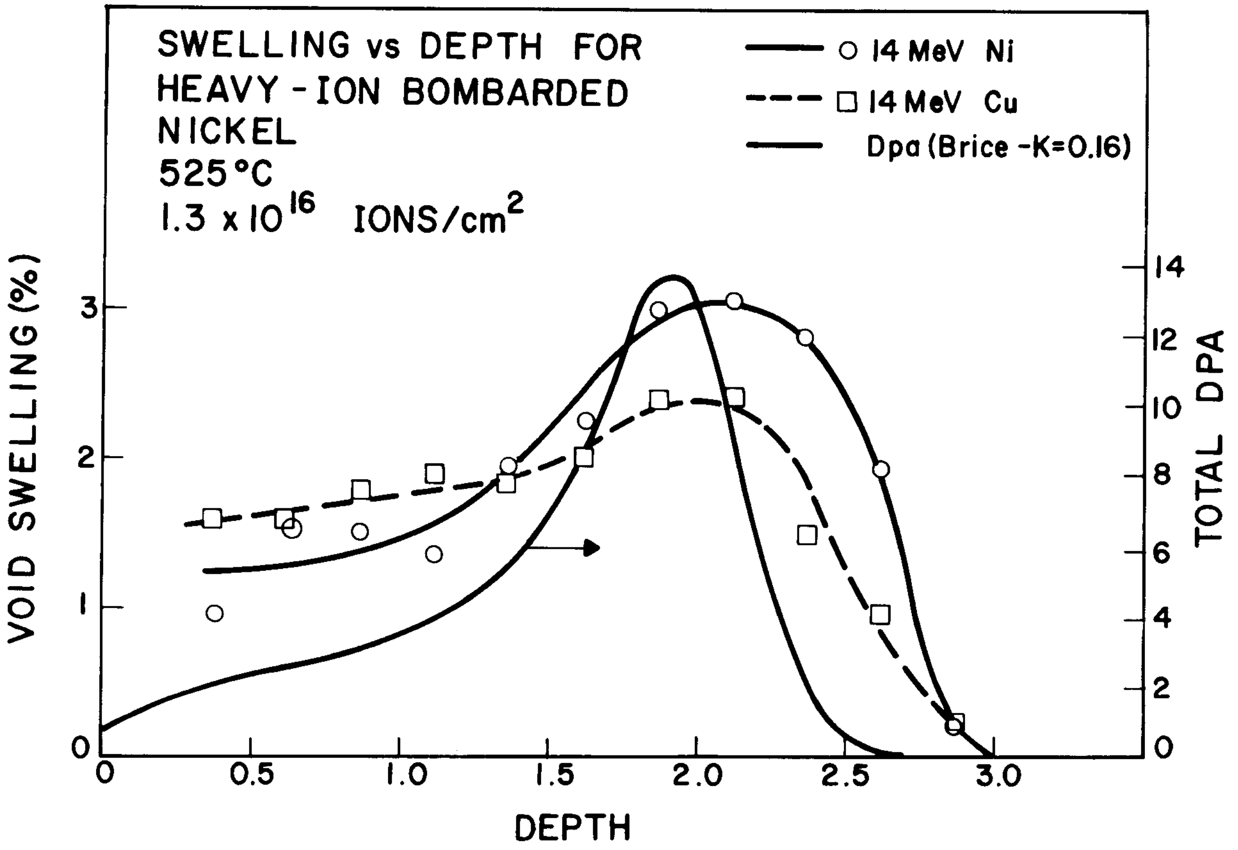

Figure 7. A comparison of the swelling profile after irradiation with 14 MeV copper ions to the profile after irradiation with 14 MeV nickel ions. The displacement curve shown is for 14 MeV nickel ions, but the 14 MeV copper ion curve would be similar.

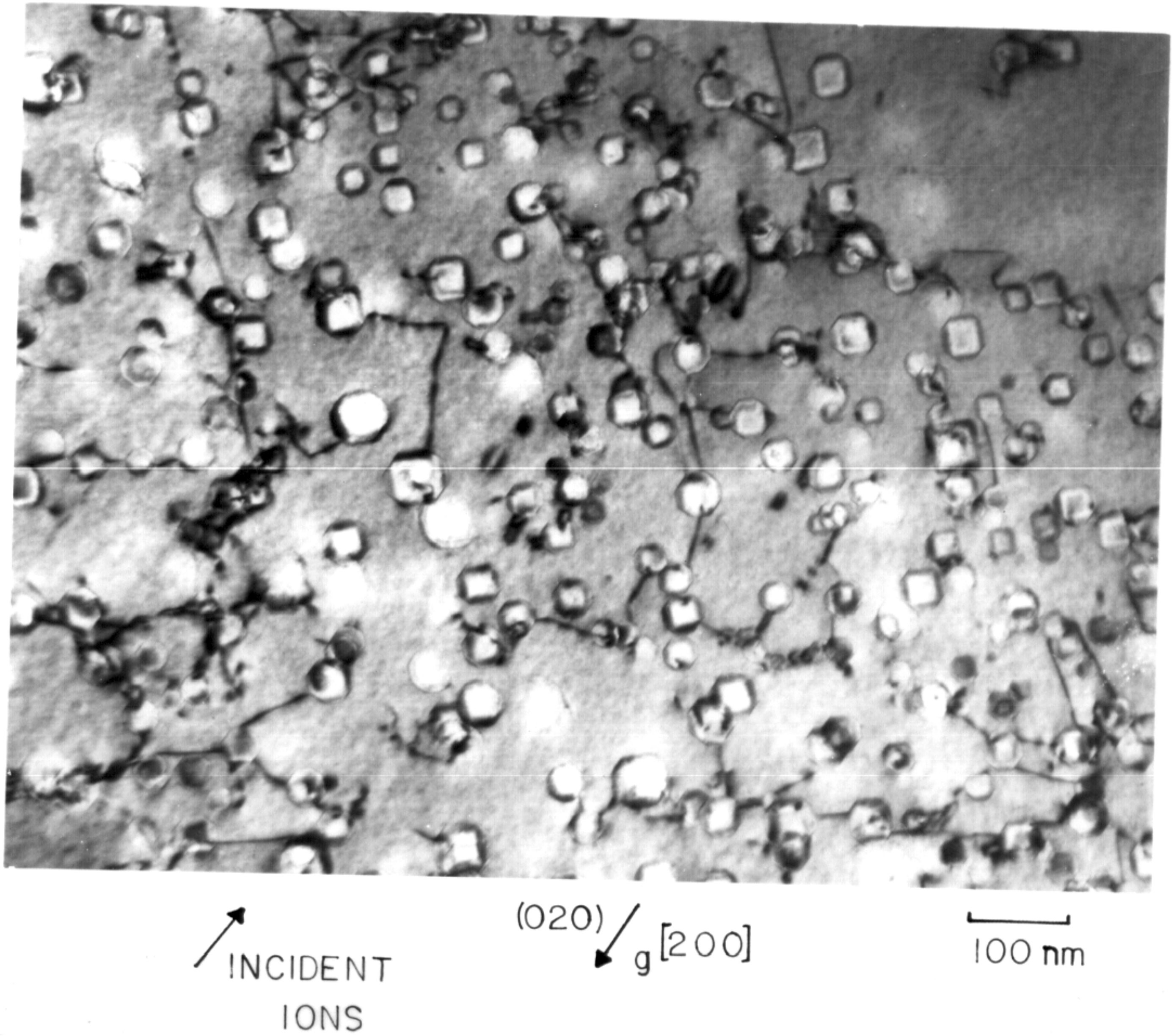

Figure 8. The dislocation structure in the end-of-range region of a nickel sample irradiated at 525°C with 14 MeV nickel ions to a fluence of 1.3 x 10^{16} ions/cm^2.

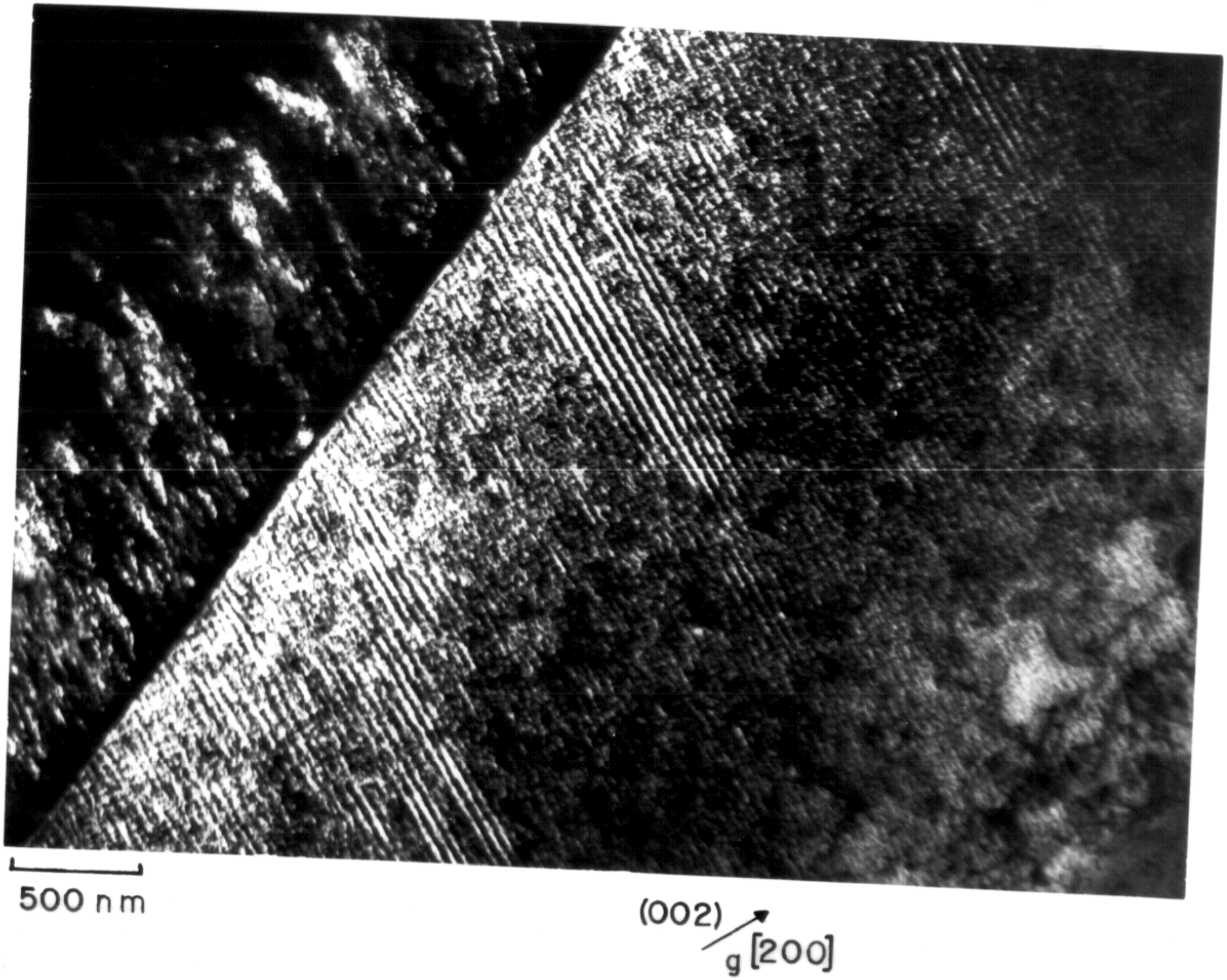

Figure 9. The loop lattice structure which formed after irradiation at 200°C with 14 MeV nickel ions to a fluence of 7 x 10^{15} ions/cm^2. The original foil surface is visible in the left half of the micrograph.

3. Defect Profile Calculations

To assist in the interpretation of the experimental results, it is useful to know not only the depth profile of the defect production rate, but also the depth profiles of the vacancy and interstitial concentrations. If the ion beam is not the same chemical species as the target material, it is also important to know the final concentration profile of the incident ions and their concentration levels. The steady-state rate equations that describe the point defect concentrations are given by

$$\nabla D_i \nabla C_i + P_i - D_i C_i k_i^2 - \alpha C_i C_v = 0 \qquad (1)$$

and

$$\nabla D_v \nabla C_v + P_v - D_v C_v k_v^2 - \alpha C_i C_v = 0 \qquad (2)$$

where the subscripts i and v refer to interstitials and vacancies respectively and the D's are diffusion coefficients, α the homogeneous recombination coefficient, P_i the interstitial production rate which includes the excess interstitials produced by the incident ion coming to rest, and P_v the vacancy production rate which includes vacancy emission from sinks.[16] The k_v^2 and k_i^2 are the total sink density terms which will generally be depth dependent.[†]

These equations were formulated in a one-dimensional manner similar to Myers, et al.,[17] and solved using a modified Gauss-Siedel iterative technique.[7] D_i, D_v and α were assumed not to vary with depth or with the local defect concentration. The defect production rates were taken from the Brice code,[9]

[†] Note that cascade collapse into vacancy loops is not included in this formulation.

and if voids were present in the microstructure, the ion range and energy loss rates were modified in the manner of Odette.[18] Figure 10 shows the vacancy and interstitial concentration obtained for the case of 14 MeV nickel ions incident on a nickel target using the parameters given in table 1. In this calculation, the dislocation density was taken as 5 x 10^9 cm/cm^3 throughout the damage region and no void sinks were included. Several features of the curves of figure 10 are important in interpreting the depth dependent microstructure of heavy ion irradiated samples. First, the front surface is a perfect defect sink, and as such it reduces both the vacancy and interstitial concentrations in this region, altering both void nucleation and void growth rates. The width of this zone will be dependent both on temperature and sink density. At this temperature and sink density, the surface has little effect on the point defect concentration beyond a depth of ~0.5 μm. Similar results near the front surface were obtained by Yoo[19] who solved these equations in their time dependent form for the case of 4 MeV nickel ion irradiation. The defect concentrations also show less variation in magnitude from the midrange to the peak region than does the defect production rate curve. This behavior is due to the non-linear response of the defect recombination rate which leads to a larger fraction of the defects recombining as the steady-state defect concentrations increase. This is illustrated by the defect rate curves of figure 11, where the fractions of defect lost to sinks, recombination and by diffusion out of depth zones are shown for the curves of figure 10. For the parameters used in this case, recombination dominates except near the front surface. Diffusion of defects beyond the production curve does give significant defect concentrations in this "undamaged" region. In this particular case the vacancy concentration at 3.0 μm was still about five orders of magnitude greater than the equilibrium value.

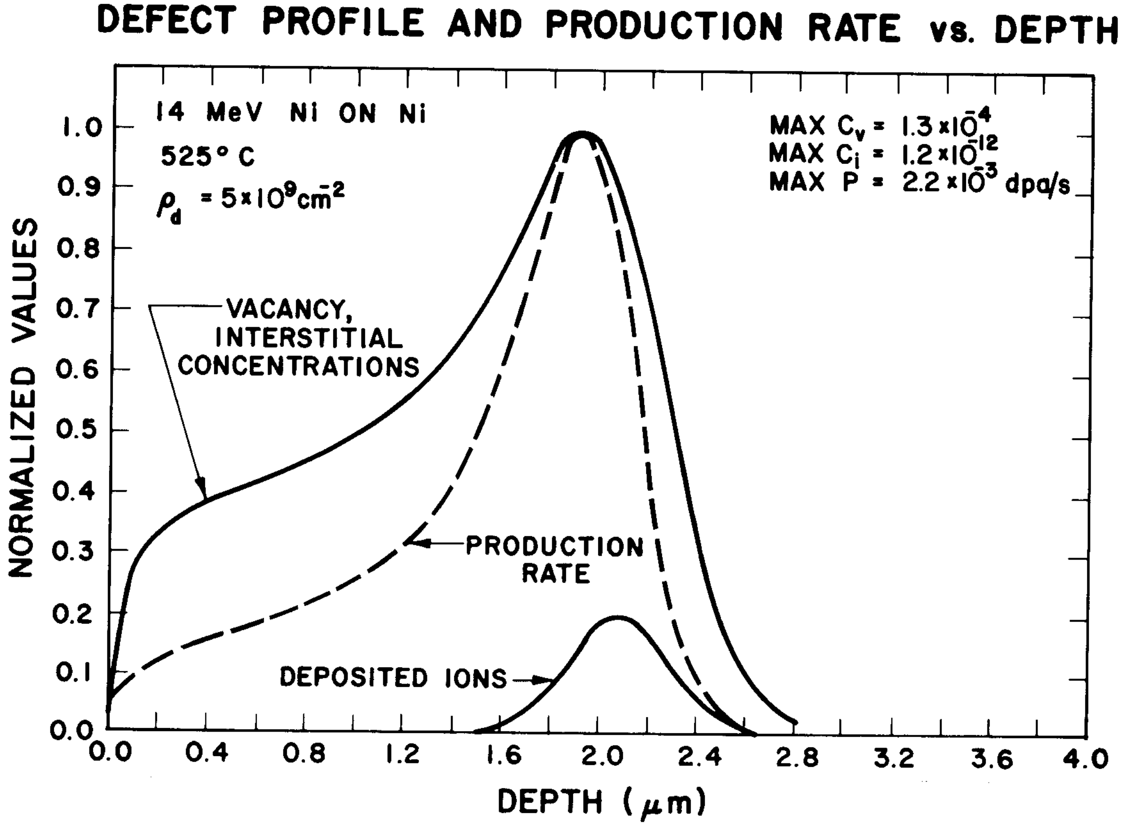

Figure 10. Vacancy and interstitial concentration profiles for 14 MeV nickel ions incident on nickel using the parameters given in Table 1. The defect production curve and the relative range distribution of the incident ions are also shown. Note that all the curves except the range curve are normalized to the peak values given in the figure.

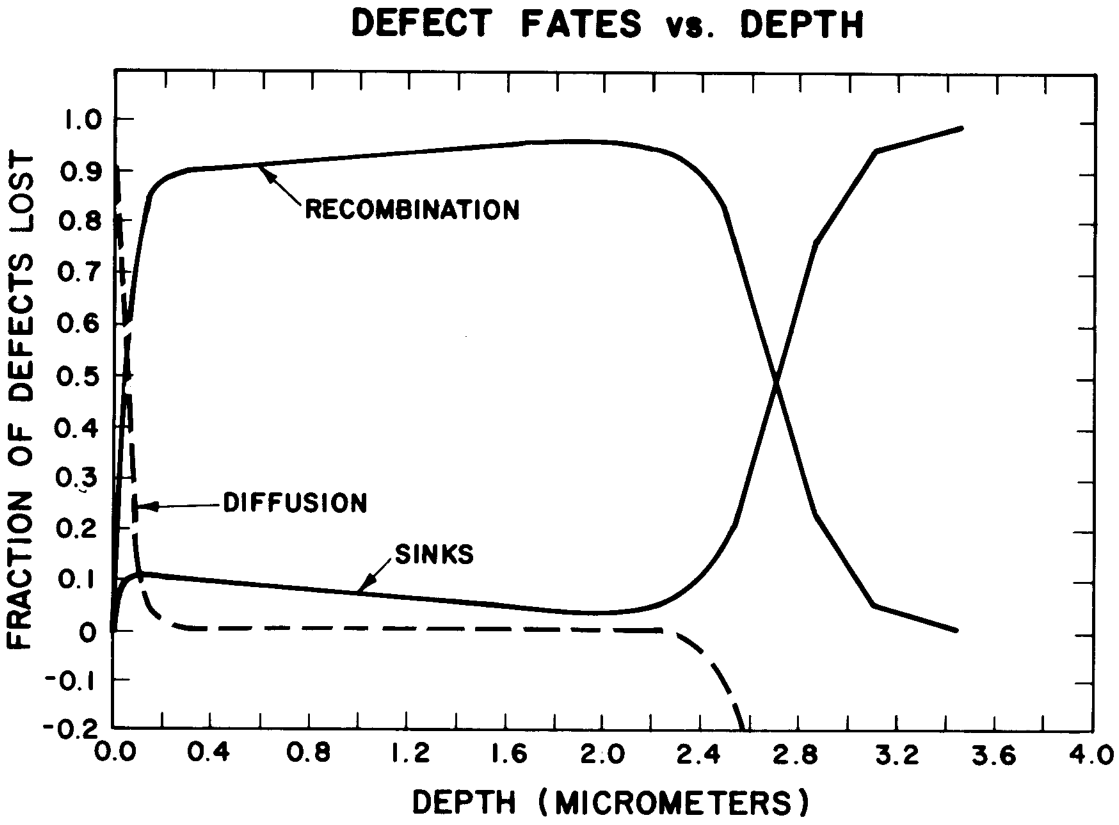

Figure 11. The fractions of defects lost by absorption at sinks, by recombination, and by diffusing from a depth region. A negative diffusion fraction is obtained when a region has a net influx of defects.

In interpreting the end-of-range microstructure of the copper ion irradiated samples, it is important to know the resultant impurity distribution. The concentration of an impurity is described by

$$\frac{\partial C_A}{\partial t} = \nabla D_A \nabla C_A + S_A \tag{3}$$

where $\underline{S}_A$ is the source term for the impurity and will be depth dependent in this case. $\underline{C}_A$ is the concentration of the impurity $\underline{A}$ in the matrix, and $\underline{D}_A$ its radiation enhanced diffusion coefficient assumed to be of the form[16]

$$D_A = \sum_K F_K D_K C_K \tag{4}$$

where the sum is over all mobile defects and defect clusters, and the $\underline{F}_K$ are correlation factors. Note that this model of radiation enhanced diffusion does not apply to interstitial impurities and neglects solute drag effects.

To model the ion irradiation case, the steady-state solutions for the vacancy and interstitial concentrations were found from equations 1 and 2 and substituted into equation (4) to give the depth dependent diffusion constant (note that mobile defect clusters such as di-vacancies were ignored in this solution). This diffusion constant was then used to solve Equation 3 in one dimension. The vacancy and interstitial correlation factors were taken as 0.78 and 0.4, respectively.[20]

Results of this calculation for 14 MeV copper ions incident on nickel are shown in figure 12. The radiation enhanced diffusion spreads the impurity predominately towards the front surface while lowering the peak concentration. At the low ion fluence typical of this study, the range of influence of the copper is still confined to the end-of-range region (figure 12a). Even in this case, however, the peak copper concentration exceeds 0.2 atomic percent. In the high fluence case (figure 12b) the copper

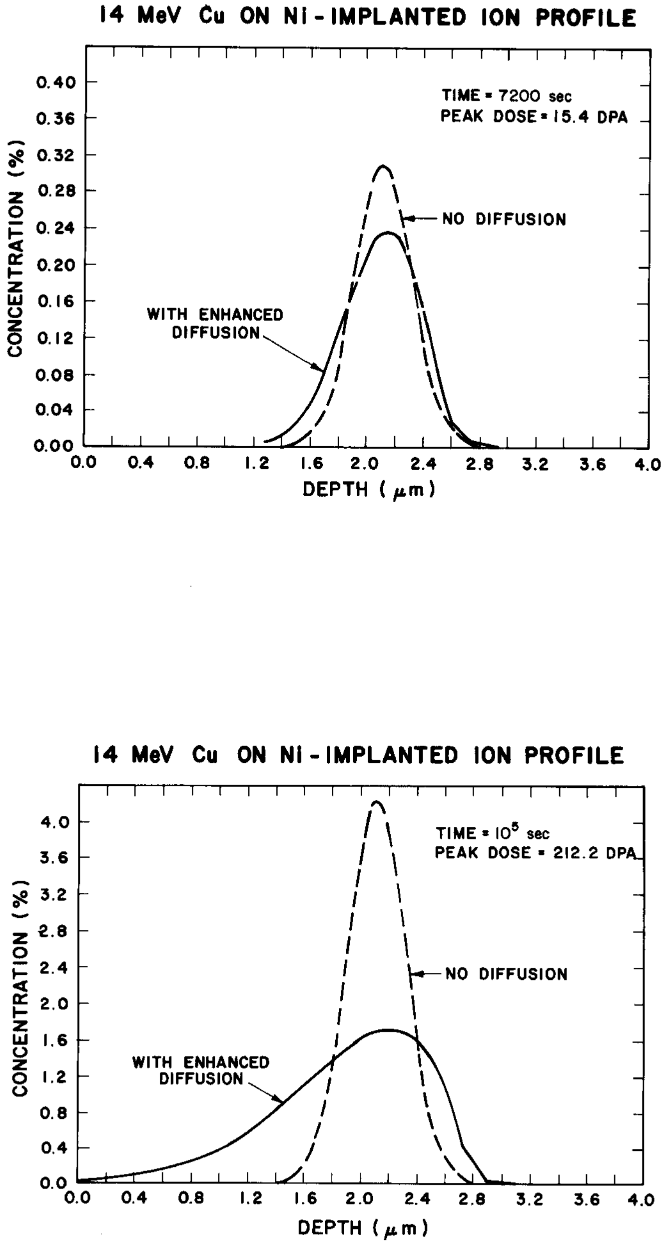

Figure 12. The final distribution of copper after irradiating an initially pure nickel foil at 525°C with 14 MeV copper ions with (solid curve) and without (dashed curve) radiation enhanced diffusion. a) After an ion fluence of 1.4 x 10^{16} ions/cm^2, b) After an ion fluence of 2 x 10^{17} ions/cm^2.

has spread throughout the damage region of the sample and reached peak concentration values exceeding 1.5 atomic percent.

4. Discussion

a. Utility of Cross Sectioning Technique

Due to the large amount of data extracted by this sample preparation technique, it is important to understand its relative strengths and weaknesses. First, for a given sample, such variables as sample heat treatment history, handling, irradiation temperature, ion flux and ion fluence are all identical. While the absolute values of void statistics are no better with this technique than in conventional sample preparation, the relative error between intervals of a given sample is reduced since microscope magnification errors are eliminated and foil thickness errors are reduced.

The interpretation of the observed structure is complicated, however, by the depth variation of features such as dose rate, total dose, impurity levels, internally generated stress levels, surface effects, and the changing primary-knock-on (PKA) spectrum. The changing differential nuclear scattering cross section for nickel on nickel is shown for two depths in figure 13a. As the ion slows down, cascades initiated by high energy PKA's are eliminated and the bulk of the displacement events are caused by lower energy, and hence smaller, cascades. This is shown more clearly in figure 13b. Over 10 percent of the displacements at the surface are caused by recoils of energy greater than 1 MeV, while there are virtually no cascades of this size at a depth of 2 μm. Within our present understanding of the radiation damage process, it has not been possible to correlate this changing PKA spectrum with any microstructural features, even though the cascade size could be expected to affect the fraction of defects surviving immediate recombination in the cascade. It is also possible that the cascade size distribution could affect such mechanisms as cascade collapse into vacancy clusters.[22]

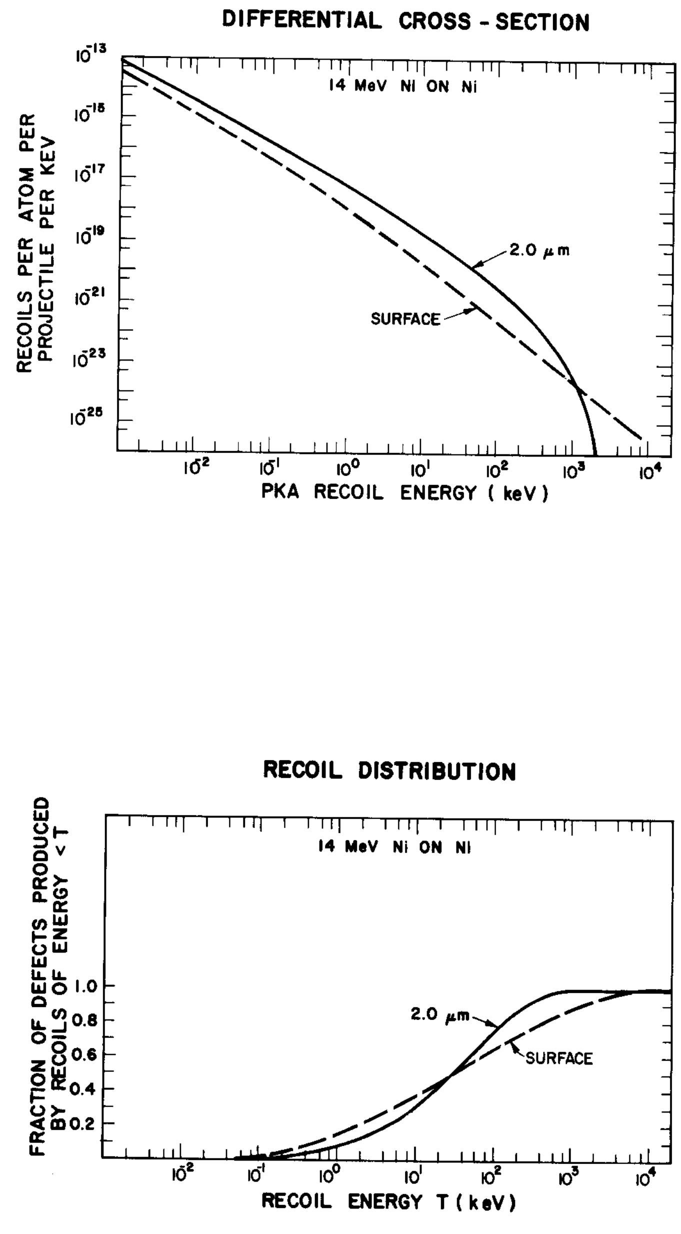

Figure 13. a) The differential scattering cross section for 14 MeV nickel ions incident on nickel at the surface and at a depth corresponding to the peak damage. b) The function F(T<) at these same two depths where F(T<) is taken after Marwick[21] and is defined as the fraction of displacements produced by recoils of energy less than T.

To avoid smearing out microstructural data that may be affected by these rapidly varying features, it was necessary to restrict the depth interval size to the relatively small value of 0.25 μm. This restriction leads to the primary problem with this technique, namely that of counting statistics. In a sample or region of a sample that has a low defect density, it may be difficult to include enough defects within an interval to give an acceptable statistical uncertainty. In this study, the samples had high enough void densities to reduce this problem except in the first one or two depth intervals, but this technique would be very limited as a method of measuring the depth dependence of defects with densities below $\approx 5 \times 10^{13}$ cm^{-3}.

b. Microstructure observations

In all samples which were examined in this study, voids were observed at depths from 15-20 percent greater than the end-of-range predicted by Brice[9] or Manning and Mueller[23]. The void density peak was also shifted beyond the predicted damage peak, but generally by only ≈10 percent. These results are consistent with earlier results[5] and with the observations of Narayan, et al.,[24,25] in heavy ion irradiated copper and nickel. The latter found better agreement between the observed defect density peak and the damage peak given by Manning and Mueller if the coefficient of the Lindhard electron energy loss term was reduced at low ion energies. By reducing the rate of electronic energy loss and correspondingly increasing the nuclear stopping power, the damage curve was shifted away from the front surface and the total number of displacements increased. There are at least three other possibilities for the observed extension of damage. An error in the range straggling calculation would extend the damage region, as would channelling of either the incident ion or a high energy recoil atom. The diffusion of vacancies into this region could lead to void formation without extending the damage curve as was shown in the calculations of figure 10.

No definite conclusion could be drawn as to the cause of the range deviation in the present work but this discrepancy should be carefully studied in future work.

The front surface of these samples showed a void denuded region of ≈100 nm at 525°C. There was a slight increase in void size immediately adjacent to the denuded region, but the amount of increase varied between samples and was generally less noticeable than the increase observed next to the void denuded regions of grain-boundaries. Due to the relatively large grain size of these samples, only a few grain boundaries were observed and these usually showed evidence of grain boundary migration during the irradiation, making an accurate comparison of denuded zone width impossible. Voids in different grains of a sample showed no noticeable difference in either the size or density profiles or in the extent of the void region. Hence from this study, there is no evidence that the grain orientation has any strong influence on the damage microstructure.

c. End-of-Range Effects

The computer calculations for the final copper concentration profile showed that for this study, the copper impurities were confined to the end-of-range region. This implies that any modifications in swelling behavior due to the presence of the copper will only occur in this region. However, the effect of copper impurities on void swelling is still somewhat uncertain. Brimhall and Kissinger[26] and Mazey and Menzinger[27] both found a 2% copper, 98% nickel alloy to swell less than a pure nickel control sample, while Smidt and Sprague[28] found a 1% copper alloy to swell more. All these workers did observe a decreased void density and an increased void size with alloying however. Brimhall and Kissinger also observed a higher density of prismatic loops in the alloy system, possibly indicating a reduction in the stacking fault energy with alloying. In contrast to these studies on dilute nickel-copper alloys, the copper injected by the irradiating beam in this study seems to have lowered both the void density and the void size. In fact the different shapes of the swelling curves of figure 7 show a reduced swelling rate in the end-of-range region of the copper irradiated sample. A more dramatic effect would be expected if the sample were irradiated to a higher damage level.

The swelling behavior of the self-ion irradiated samples (figure 7) does not directly follow the displacement curve. Specifically, the variation from mid-range to the peak swelling value is much smaller than the corresponding variation in the damage curve. In figure 14, this swelling curve is shown plotted along with the net flux of vacancies into a distribution of test voids calculated from the data of figure 11. This "growth fluid"[‡] is a valuable aid in interpreting void growth data. (While these curves are not exactly equivalent in that the growth fluid is a swelling rate, the discrepancy is minor since the small incubation dose of pure materials allows one to approximate a swelling rate by a single swelling value.) The good qualitative agreement between these curves indicate that the reduced swelling value per dpa in the peak region can be at least partially explained by the enhanced recombination and the excess interstitials deposited in the end-of-range region. Note that this result is similar to that obtained by the internal temperature shift at temperatures below the peak swelling temperature as described by Garner and Guthrie.[3] In calculating the growth fluid, however, a void distribution was assumed, while the experimental temperature shift includes the temperature and rate variations in void nucleation.

[‡] The growth fluid is defined by Garner[3] as $D_vC_v-D_iC_i-D_vC_v^*$, where C_v^* is the vacancy concentration at the void surface with no irradiation.

5. Conclusions

The cross sectioning method of post-irradiation sample preparation for heavy ion bombarded nickel has proven to be a valuable aid in understanding the irradiation microstructure produced by this simulation technique. This study has found:

1) The swelling rate per dpa in the end-of-range region was decreased significantly for both copper and nickel ion irradiations compared to the mid-range values. The copper ion irradiated sample displayed a somewhat lower variation than the self-ion bombarded specimen.

2) Calculations of the steady-state defect concentrations showed a decreased swelling rate at the end-of-range of the incident ions due to the higher recombination rate.

3) By modeling the radiation enhanced diffusion of the implanted copper ions, it was shown that for the samples of this study, the copper was confined to the end-of-range region.

4) A void denuded region of ≈100 nm was observed at the front surface at 525°C, and voids were observed at depth ≈15 percent greater than the extent of the predicted damage curve.

5) A loop lattice with a lattice spacing of 40 nm was observed after irradiation at 200°C, and the lattice spacing was not found to be dose rate or otherwise depth dependent.

6. Acknowledgements

This research was sponsored by the Department of Energy, Division of Magnetic Fusion Energy, under contract number ET-78-S-02-4640. The authors are grateful to the University of Wisconsin Nuclear Physics Group for use of the tandem accelerator and its facilities.

References

1. G.L. Kulcinski, Applications of Ion Beams to Metals, Plenum Press, NY, P. 613 (1974).

2. W.G. Johnston and J.H. Rosolowski, Applications of Ion Beams to Materials, 1975, P. 228 (1975).

3. F.A. Garner and G.L. Guthrie, Int. Conf. on Rad. Effects and Tritium Technology for Fusion Reactors, CONF-750989 P. I-491 (1976).

4. F. Menzinger and F. Sacchetti, J. Nucl. Mat. 57, P. 193 (1975).

5. J.B. Whitley, P. Wilkes, G.L. Kulcinski, UWFDM-159, Nuc. Engr. Dept., Madison, Wis. (1976).

6. R.A. Spurling and C.G. Rhodes, J. Nucl. Mat. 44, P. 341 (1972).

7. J.B. Whitley, G.L. Kulcinski, UWFDM-241, Nuc. Engr. Dept., Madison, Wis. (1978).

8. H.V. Smith and R.G. Lott, Nuc. Ins. and Methods 143, P. 125 (1977).

9. D.K. Brice, SAND75-0622, Sandia Laboratories, Albuquerque, New Mexico, (July 1977).

10. T.D. Ryan, Ph.D. Thesis, Univ. of Mich. (1975).

11. Recommended practice for neutron damage simulation by charged particle irradiation, E521-76 (Prepared under ASTM Committee E-10, Subcommittee E10.08) (1974).

12. T.M. Rodgers, Handbook of Practical Electroplating, P. 225, Macmillian Co., NY (1959).

13. G.L. Kulcinski and J.L. Brimhall, Effects of Rad. on Substructure and Mech. Prop. of Metal and Alloys, ASTM STP 529, (1973) P. 258.

14. J.A. Sprague, J.E. Westmoreland, F.A. Smidt, Jr., and P.R. Malmberg, J. Nuc. Mat. 54, P. 286 (1974).

15. J.E. Westmoreland, J.A. Sprague, F.A. Smidt, Jr., and P.R. Malmberg, Rad. Eff. 26, P. 1 (1975).

16. A.D. Brailsford and R. Bullough, J. Nuc. Mat. 44, P. 121 (1972).

17. S.M. Myers, D.E. Amos, D.K. Brice, J. App. Physics, No.5, P. 1812 (1976).

18. G.R. Odette, D.M. Schwartz, and A.J. Ardell, Rad. Eff. 22, P. 217 (1974).

19. M.H. Yoo, J. Nuc. Mat. 68, P. 193 (1977).

20. Y. Adda, M. Beyeler, and G. Brebec, Thin Solid Films 25. P. 107 (1975).

21. A.D. Marwick, Consultant Symposium on The Physics of Irradiation Produced Voids, Harwell, P. 39 (1975).

22. R. Bullough, Consultant Symposium on The Physics of Irradiation Produced Voids, Harwell, P. 275 (1975).

23. I. Manning and G.P. Mueller, Computer Phys. Comm. 7, P. 85 (1974).

24. J. Narayan and O.S. Oen, J. Nuc. Mat. 66, P. 158 (1977).

25. J. Narayan, O.S. Oen, and T.S. Noggle, J. Nuc. Mat. 71, P. 160, (1977).

26. J.L. Brimhall and H.E. Kissinger, Rad. Eff. 15, P. 259 (1972).

27. D.J. Mazey and F. Menzinger, J. Nuc. Mat. 48, P. 15 (1973).

28. F.A. Smidt and J.A. Sprague, NRL Mem. Report #2998, P. 39 (March, 1975).

Table 1.

Input Parameters Used in Solving Eq. 1 and 2.

Most Material Parameters are from Ref. 10

Temperature	525°C
Dislocation density	5×10^9 cm^{-2}
Surface energy	1000 mJ/m^2 (erg/cm^2)
Vacancy migration energy	1.38 eV
Interstitial migration energy	0.15 eV
Vacancy formation pre-exponential	4.48
Interstitial formation pre-exponential	5.0
Vacancy diffusion coefficient pre-exponential	0.062 cm^2/s
Interstitial diffusion coefficient pre-exponential	0.12 cm^2/s
Vacancy formation energy	1.39 eV
Interstitial formation energy	4.08 eV
Recombination factor, α/D_i	1×10^{15} cm^{-2}
Dislocation bias	2.0%
Ion flux	2×10^{12} $ions/cm^2/s$